DISCOVERY OF IMPACT ARMORING ON (101955) BENNU. E. B. Bierhaus[1], D. Trang[2], R. T. Daly[3], C. A. Bennett[4], O. S. Barnouin[3], K. J. Walsh[5], R.-L. Ballouz[4], W. F. Bottke[5], K. N. Burke[4], M. E. Perry[3], E. R. Jawin[6,7], D. S. Lauretta[4]. [1]Lockheed Martin Space, [2]Hawai'i Inst. of Geophysics and Planetology, Univ. of Hawai'i at Mānoa, [3]Johns Hopkins Univ. Applied Physics Laboratory, [4]Lunar and Planetary Laboratory, Univ. of Arizona, [5]Southwest Research Inst., [6]Smithsonian Inst. Nat. Museum of Natural History, [7]Smithsonian Inst. Nat. Air and Space Museum.

Introduction: Impact cratering is ubiquitous across the Solar System [1] and is a major process driving surface evolution on asteroids [2-5]. Impact-scaling relationships [e.g. 6] relate properties of the impactor, target surface, and resulting crater, and are necessary to translate an observed crater population into a crater-retention age (the age recorded by the craters themselves [e.g. 7]). Crater-retention ages are thus sensitive to the accuracy of the scaling relationships.

The Hayabusa mission to the rubble-pile asteroid Itokawa observed craters that contrast morphologically with those on larger asteroids and planetary surfaces [5], and prompted investigations of impact cratering on rubble-pile surfaces [8-10].

Experiments [9] suggest that when impactor energy is comparable to or smaller than the disruption energy of the target surface particle — a condition common to rubble piles — crater formation in the bulk asteroid surface is inhibited or prevented by an "armoring" effect (though a pit crater may form on the target particle [11]).

The global coverage and high spatial resolution of the data collected by the OSIRIS-REx spacecraft at the rubble-pile asteroid Bennu [12] make it possible to test this impact-armoring paradigm. Here we describe a complete, global database of Bennu's crater population and evaluate the ability of armoring scaling to explain the observed crater size-frequency distribution. We find that impact armoring explains the unusual character of Bennu's small-crater size-frequency distribution (SFD), and corresponds to a young crater-retention age for small craters.

Impact craters on Bennu: We identified and measured 1560 craters using OSIRIS-REx Camera Suite (OCAMS [13]) images, and digital terrain models (DTMs [14]) generated from OSIRIS-REx Laser Altimeter (OLA [15]) data. We also engaged citizen scientists for image-based crater identification [16].

Larger craters on Bennu are circular or elliptical features with raised rims and/or depressed floors (Fig 1A). Smaller craters (<~10 m diameter) often lack raised rims; however, they can have a surrounding ring of boulders and/or exhibit a particle-size contrast between their interior and exterior (Fig. 1B), which often correspond to spectrophotometric changes in visible wavelengths [17].

Bennu's crater SFD: The differential form of Bennu's crater population makes a "fishhook" shape (Fig. 2). (The differential form is $N_d = dN/(dD\,A)$, where dN is the number of craters in diameter range dD, and A is the surface area; unlike the cumulative SFD, the differential is a direct representation of the number of craters present at any given size.) The number of craters increases with decreasing diameter until 2–3 m, at which point the abundance rapidly decreases to zero. We explore several explanations for the decrease.

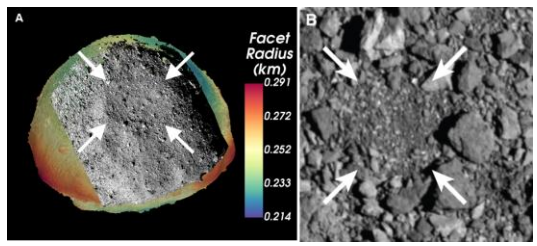

Fig. 1. Examples of large and small craters on Bennu. (A) a 141-m-diameter crater, and (B) a 4 m diameter crater. White arrows in both frames indicate the crater location. Adapted from [18].

Completeness limit. Previous analysis [19] suggested a typical ~10 pixel completeness limit, below which features may be identified, but finite resolution leads to incomplete identification. The decrease in craters for diameters < 3 m in Fig. 2 corresponds to 46 PolyCam pixels and 23 DTM post-spacings; this is about 4 and 2 times greater, respectively, than the 10-pixel completeness limit. The lighting and viewing geometries of these images have moderate incidence angles for shadowing and low emission angles, the preferred combination for identification and morphological analysis. Thus, we eliminate finite spatial resolution of the data as the cause for the decrease in crater density below ~3 m diameter.

Seismic shaking. Seismic shaking by impact has been invoked [20] to explain erosion of craters on asteroids. Modeled effects apply erasure efficiencies sufficient for more frequently-formed smaller craters to erase larger craters, leading to fewer observable craters. However, the SFD still results in a population with an increasing number of smaller craters, contrary to our measurements. Also, observations [21] from the region immediately around the artificial crater created by the Hayabusa2 mission on Ryugu indicate inefficient translation of impact energy into seismic shaking, limiting the effect to local area around the impact site.

Mass wasting. Localized regions of recent mass movement have been observed on Bennu that appear

correlated with recent changes in spin rate and slope instabilities [22]. If these mass movements erased small craters, the small-crater abundance would be anti-correlated with slope; however, we find the spatial density of craters 1–3 m in diameter (i.e., in the fishhook transition from increasing to decreasing number density) are not correlated with regions of high slope. Crater depth-diameter ratios are not correlated with slope either [23], contrary to expectations if mass wasting caused infilling of small craters. Thus, although mass movement may erase some small craters immediately adjacent to high-slope regions, it cannot account for the global under-abundance of small craters.

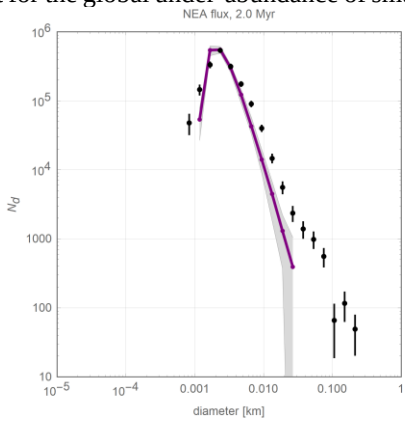

Fig. 2. Crater SFD of Bennu in differential format. Black points are observations, the purple data are the median results from 100 simulations of a 2 Myr NEA-flux dominated age, and the gray-shaded band represents the range of 99% of the simulations. Adapted from [18].

Impact armoring: We hypothesize that the fishhook shape of the crater SFD at small diameters is due to impact armoring. To evaluate this hypothesis, we developed a model derived from a rubble-pile impact scaling relationship [9] (hereafter, TS2018 scaling) to compare with observations. A possible outcome for an impactor using TS2018 scaling is a failure to make a crater in the bulk asteroid surface. Whether a crater forms, and the diameter of the resulting crater if created, depends on the sizes of both the impactor and target boulder. Thus, to model crater production, we generated both impactor and target particle sizes via a Monte Carlo simulation. To determine impactor sizes, we used estimates of the impactor flux both in the main belt and in near-Earth space because Bennu formed as a main-belt asteroid (MBA) and evolved to be a near-Earth asteroid [24] (NEA). To determine boulder sizes, we used the observed boulder SFD [25-26]. Because modeling the crater population for a given surface age is probabilistic with this technique, we generated 100 cases for each age to develop statistics on the potential range of outcomes. We find that this model recreates the fishhook shape (Fig. 2).

Fitting the height of the fishhook provides an estimate of the crater-retention age for small diameters. Based on minimum residuals, we find a small-crater NEA-flux age of 1.6–2.2 Myr. This is consistent with an age derived from examining craters in boulders [11], and color properties of small craters [17]. The time needed to generate the large craters with an NEA flux is >100 Myr, significantly larger than Bennu's estimated time as an NEA [27], meaning the large craters are a residual crater population from Bennu's time in the main belt. Using a main belt flux, we find a large-crater-retention age of 10-65 Myr, younger than a previous estimate [28] that used strength-scaling to estimate a maximum age for the largest craters.

Acknowledgments: This material is based upon NASA Contracts NNM10AA11C and NNG12FD66C issued through the New Frontiers Program. The OLA instrument and Canadian science support was provided by contracts with the Canadian Space Agency. We thank the entire OSIRIS-REx Team.

References: [1] Melosh, H.J. (1989). Oxford University Press. [2] Chapman, C.R., et al. (2002). *Icarus*, v. 155, 104-118. [3] Chapman, C.R., et al. (1996a). *Icarus*, v. 120, 77-86. [4] Hirata N. et al. (2020). *Icarus*, v. 338. [5] Hirata, N., et al. (2009). *Icarus*, v. 200, 486-502. [6] Holsapple, K.A. (1993). *Ann. Rev. of Earth and Planet. Sci*., v. 21, pp. 333-373. [7] Shoemaker E. M. (1965). In *The nature of the lunar surface*, Johns Hopkins University Press. pp. 23–77. [8] Durda, D.D., et al. (2011). *MAPS*, v. 46, 149-155. [9] Tatsumi, E. and Sugita, S. (2018). *Icarus*, v. 300, 227-248. [10] Barnouin, O.S., et al. (2019). *Icarus*, v. 325, 67-83. [11] Ballouz, RL., et al. (2020) *Nature*, 587, 205–209. [12] Lauretta, D. S., et al. (2021) In Sample Return Missions, ed. Longobardo, A. (Elsevier), 163–194. [13] Rizk, B. et al. (2018). *SSR*, v. 214, 26. [14] Barnouin, O. S., et al. (2020). *Planet. Space Sci.*, 104764. [15] Daly, M.G., et al. (2017). *SSR*, v. 212, 899-924. [16] Gay, P.L., et al. (2020) https://github.com/CosmoQuestX/CSB7.0. [17] DellaGiustina, D. N. et al. (2020). *Science* 370, eabc3660. [18] Bierhaus et al., *Nat. Geosci*, in revision. [19] Robbins, S.J., et al. (2014) *Icarus*, 234, 109-131. [20] Richardson, J.E., et al. (2020) *Icarus*, 347, 113811. [21] Honda, R. et al. (2021). *Icarus*, 366, 114530. [22] Jawin E.R., et al. (2020) *JGR Planets*, 125(9), E06475. [23] Daly, T., et al. (2020) *GRL*, 47, eGL089672. [24] Bottke, W. F. et al. (2020) *Astron. J.* 160, 14. [25] DellaGiustina, D.N., et al. (2019 *Nat Astron.* 3, 341–351. [26] Burke, K. et al. (2021) *Remote Sens*. 2021, 13(7), 1315. [27] Bottke, W.F. et al. (2015). *Icarus*, 247, 191-217. [28] Walsh, K.J., et al. (2019) *Nat. Geosci*. 12, 242–246.